

Key words: heart-valve dynamics, elastic waves, arbitrary Lagrangian Eulerian method, finite element method, fluid-structure interaction, goal-oriented mesh adaption
2010 MSC: 74F10, 74B20, 65N30, 65M60, 35Q74

THOMAS WICK *

GOAL-ORIENTED MESH ADAPTIVITY FOR FLUID-STRUCTURE INTERACTION WITH APPLICATION TO HEART-VALVE SETTINGS

We apply a fluid-structure interaction method to simulate prototypical dynamics of the aortic heart-valve. Our method of choice is based on a monolithic coupling scheme for fluid-structure interactions in which the fluid equations are rewritten in the ‘arbitrary Lagrangian Eulerian’ (ALE) framework. To prevent the backflow of structure waves because of their hyperbolic nature, a damped structure equation is solved on an artificial layer that is used to prolongate the computational domain. The increased computational cost in the presence of the artificial layer is resolved by using local mesh adaption. In particular, heuristic mesh refinement techniques are compared to rigorous goal-oriented mesh adaption with the dual weighted residual (DWR) method. A version of this method is developed for stationary settings. For the nonstationary test cases the indicators are obtained by a heuristic error estimator, which has a good performance for the measurement of wall stresses. The results for prototypical problems demonstrate that heart-valve dynamics can be treated with our proposed concepts and that the DWR method performs best with respect to a certain target functional.

1. Introduction

A major fraction of mortalities in industrialized countries is represented by cardiovascular diseases. For this reason, there is an increasing demand from the medical community for rigorous and quantitative investigations of the human cardiovascular system. However, the complexity of the circulatory system makes modeling and simulation challenging because there are many fundamental factors that must be taken into account.

In this work, we focus on the main component of the circulatory system: the heart. More specifically, we are interested in modeling and simulation of the aortic heart-valve, which ejects oxygenated blood from the left ventricle

* *Institute of Applied Mathematics, University of Heidelberg, INF 293/294, 69120 Heidelberg, Germany; E-mail: thomas.wick@ivr.uni-heidelberg.de*

in the aorta. Such processes imply the interaction of blood with both the myocardium and the vessel walls. The mathematical method of choice to construct appropriate models and simulations is the fluid-structure interaction approach. Beyond that, fluid-structure interactions have significant influence in biomedical engineering [1-4].

However, mathematical modeling and numerical simulations of processes of the human circulatory system remain challenging. For instance, it remains to find appropriate structural boundary conditions on the outflow section in a compliant blood vessel with elastic walls [5, 6]; and the many references cited therein. An approach to resolve aortic heart-valve related questions is studied in [7, 8]. There, the influence of different damping parameters and various lengths of the artificial layer is analyzed. Beside the fact that the choice of the artificial layer is artificial, it might nevertheless be used for clinical applications because the value of the parameters can be obtained with comparisons with clinical data. On the other hand, numerical simulations have a high computational cost for three-dimensional simulations of the whole cardiovascular system. Consequently, such simulations are still challenging; despite further development of hardware-oriented code and parallel programming in the last years. Thus, the final goals to deliver patient specific information and comparisons of simulations with clinical data remain a tough task.

Heart-valve dynamics are handled with different concepts. Usually, they are considered as fluid-structure interaction problems that can be solved with different solution approaches [9-13]. Presently, the predominant method for treating (realistic) heart-valve simulations in the biomedical context are fictitious domain methods (see, e.g., [14]). In the present study, we use the 'arbitrary Lagrangian-Eulerian' framework (ALE) that is frequently used in the literature to model fluid-structure interaction problems. The advantage of the ALE method is a common mesh for the coupled problem, the exact representation of the fluid-structure interface (interface-tracking), and consequently clearly defined quadrature rules in each mesh cell. To track the interface has the advantage to control the mesh resolution near the interface (i.e., to refine the mesh geometrically). By construction, the ALE approach is not capable to model topological changes, which occur when two valves touch each other. However, this point is of less importance in our studies.

The problem is solved with a monolithic solution algorithm because the well-known added-mass effect has to be overcome, which occurs when the density of the fluid and the structure are of same order, such as in hemodynamics [15]. In addition, a closed setting for the equations is necessary for rigorous goal-oriented error estimation [16], which is the goal of this work.

In this work, we shall give some further input to resolve the difficulties that are related to the computational cost; but more from the prototypical point of view. Namely, we investigate efficient methods to reducing the computational cost for finite element simulations, without the necessity to develop a fully parallelized programming code. Our solution approach is based on the development of efficient strategies for adaptive mesh refinement that is applied to heart-valve related dynamics.

Moreover, in the presence of an artificial layer that is intended to absorb the structure waves, the major disadvantage of our approach is a higher computational cost because we solve both the full fluid equations and the full structure equations in that artificial domain. To overcome this drawback, we could solve either reduced equations in the artificial layer, or using an initial coarser mesh in the artificial part, or refining the mesh automatically during the solution process. We present a combination of the two latter issues. On the one hand, we coarsen the initial mesh manually in the artificial domain. Furthermore, we use refinement indicators that are obtained by measuring the smoothness of the discrete solutions. These indicators are achieved in a heuristic manner. To substantiate (or disprove) whether this refinement technique also holds for rigorous a posteriori error estimation, we discuss the dual weighted residual (DWR) method (introduced in [16]) for stationary valve settings. Using this method, the primal residuals are weighted with dual weights while solving an associated adjoint problem. The DWR approach for fluid-structure interaction has also been investigated by others [17-21].

The paper is organized as follows: In Section 2, we describe the equations for both the fluid and the structure, including a damped hyperbolic equation. Afterwards, we formulate the problem in a monolithic setting. Section 3 is devoted to a brief description of the discretization process and adaptive mesh refinement. The temporal discretization is based on the shifted Crank-Nicolson scheme; for the spatial discretization a Galerkin finite element approach is utilized. A Newton method is applied to solve the nonlinear system. Moreover, we introduce the DWR method that is used as an indicator for goal-oriented mesh adaptation. In the last section, numerical tests are presented to exemplify our proposed methods. The parameters for both the material and the geometry are taken from the literature and were discussed with a medical doctor.

2. Fluid-structure problem

We introduce some notation and study the interaction of an incompressible Newtonian fluid and a structure of hyperbolic type [5]. The choice of the fluid model is reasonable because the Reynolds number ~ 4500 [22] is

high enough such that we are allowed to neglect non-Newtonian fluid flow effects. The choice of the structure model is also correct for the simulation of nonstationary problems. As already mentioned in the introduction, we use a damped wave equation in an artificial layer to prevent back-traveling structure waves. This choice is arbitrary and it requires further investigations from the physical point of view. Moreover, we neglect a pre-stressed structure configuration and viscoelastic structural effects [23-25]. For instance, living tissues must be modeled as composite reinforced fibers and that they account for pre-stressed configurations [24]. Nevertheless, the simple models already provide useful numerical information and they facilitate the development of reliable adaptive mesh refinement.

2.1. Notation

We denote with $\Omega \subset \mathbb{R}^d$, $d = 2, 3$, the domain of the fluid-structure interaction problem. This domain is supposed to be time independent but consists of two time dependent subdomains $\Omega_f(t)$ and $\Omega_s(t)$. The interface between both domains is denoted with $\Gamma_i(t) = \partial\Omega_f(t) \cap \partial\Omega_s(t)$. The initial (or later reference) domains are denoted with $\widehat{\Omega}_f$ and $\widehat{\Omega}_s$, respectively, with the interface $\widehat{\Gamma}_i$. Furthermore, we denote the outer boundary with $\partial\widehat{\Omega} = \widehat{\Gamma} = \widehat{\Gamma}_D \cup \widehat{\Gamma}_N$ where $\widehat{\Gamma}_D$ and $\widehat{\Gamma}_N$ denote Dirichlet and Neumann boundaries, respectively.

We adopt standard notation for the usual Lebesgue and Sobolev spaces [26]. Let $X \subset \mathbb{R}^d$, $d = 2, 3$ be a time independent domain. For instance, we later use $X := \widehat{\Omega}_f$ or $X := \widehat{\Omega}_s$. We indicate with $L^p(X)$, $1 \leq p \leq \infty$ the standard Lebesgue space that consists of measurable functions u , which are Lebesgue-integrable to the p -th power. The set $L^p(X)$ forms a Banach space with the norm $\|u\|_{L^p(X)}$. Specifically, we define $H_0^1(X) = \{v \in H^1(X) : v = 0 \text{ on } \Gamma_D \subset \partial X\}$. Vector-valued and tensor-valued variables and corresponding functional spaces are denoted in bold letters. We use frequently the short notation

$$\widehat{\mathbf{V}}_X := H^1(X), \quad \widehat{\mathbf{V}}_X^0 := H_0^1(X)$$

and

$$\begin{aligned} \widehat{\mathcal{L}}_X &:= L^2(X), & \widehat{\mathcal{L}}_X^0 &:= L^2(X)/\mathbb{R}, \\ \widehat{\mathcal{L}}_X &:= L^2(X), & \widehat{\mathcal{L}}_X^0 &:= L^2(X)/\mathbb{R}. \end{aligned}$$

Specifically, we introduce the trial and the test space for the velocity variables in the fluid domain,

$$\widehat{\mathbf{V}}_{f,\widehat{v}}^0 := \{\widehat{\mathbf{v}}_f \in H_0^1(X) : \widehat{\mathbf{v}}_f = \widehat{\mathbf{v}}_s \text{ on } \widehat{\Gamma}_i\}.$$

Moreover, we introduce the trial and the test spaces for the artificial displacement (for the mesh moving) in the fluid domain,

$$\begin{aligned}\hat{\mathbf{V}}_{f,\hat{\mathbf{u}}}^0 &:= \{\hat{\mathbf{u}}_f \in H_0^1(X) : \hat{\mathbf{u}}_f = \hat{\mathbf{u}}_s \text{ on } \widehat{\Gamma}_i\}, \\ \hat{\mathbf{V}}_{f,\hat{\mathbf{u}},\widehat{\Gamma}_i}^0 &:= \{\hat{\boldsymbol{\psi}}_f \in H_0^1(X) : \hat{\boldsymbol{\psi}}_f = \hat{\boldsymbol{\psi}}_s \text{ on } \widehat{\Gamma}_i \subset \partial X\}.\end{aligned}$$

2.2. The coupled problem

Let $\hat{\mathcal{A}}_f(\hat{\mathbf{x}}, t) : \widehat{\Omega}_f \times I \rightarrow \Omega_f(t)$ be a piecewise continuously differentiable invertible mapping. We define the physical unknowns $\hat{\mathbf{v}}_f$ and \hat{p}_f in $\widehat{\Omega}_f$ with the help of

$$\hat{\mathbf{v}}_f(\hat{\mathbf{x}}, t) = \mathbf{v}_f(x, t) = \mathbf{v}_f(\hat{\mathcal{A}}_f(\hat{\mathbf{x}}, t), t), \quad \hat{p}_f(\hat{\mathbf{x}}, t) = p_f(x, t) = p_f(\hat{\mathcal{A}}_f(\hat{\mathbf{x}}, t), t).$$

Then, with

$$\widehat{\mathbf{F}} := \widehat{\nabla} \hat{\mathcal{A}}_f, \quad \hat{J} := \det \widehat{\mathbf{F}},$$

we get the standard relations

$$\nabla \mathbf{v}_f = \widehat{\nabla} \hat{\mathbf{v}}_f \widehat{\mathbf{F}}^{-1}, \quad \partial_t \mathbf{v}_f = \partial_t \hat{\mathbf{v}}_f - (\widehat{\mathbf{F}}^{-1} \partial_t \hat{\mathcal{A}}_f \cdot \widehat{\nabla}) \hat{\mathbf{v}}_f, \quad \int_{\Omega_f} f(\hat{\mathbf{x}}) dx = \int_{\widehat{\Omega}_f} \hat{f}(\hat{\mathbf{x}}) \hat{J} d\hat{\mathbf{x}}.$$

The boundary of $\widehat{\Omega}_f$ is divided into three non-overlapping parts $\partial \widehat{\Omega}_f = \widehat{\Gamma}_{f,D} \cup \widehat{\Gamma}_{f,N} \cup \widehat{\Gamma}_i$, where $\widehat{\Gamma}_i$ denotes later the interface and it coincides with $\widehat{\Gamma}_{f,N}$ in the case of pure fluid problems. We prescribe

$$\begin{aligned}\hat{\mathbf{u}} &= \hat{\mathbf{u}}_D, \quad \text{and} \quad \hat{\mathbf{v}} = \hat{\mathbf{v}}_D \quad \text{on } \widehat{\Gamma}_{f,D}, \\ \hat{J} \widehat{\boldsymbol{\sigma}}_f \widehat{\mathbf{F}}^{-T} \hat{\mathbf{n}}_f &= \hat{\mathbf{g}} \quad \text{on } \widehat{\Gamma}_{f,N}.\end{aligned}$$

Let $\hat{\mathbf{v}}_f^D$ a suitable extension of Dirichlet inflow data. Then, the variational form in $\widehat{\Omega}_f$ reads:

Problem 2.1 (Practicable ALE-fluid problem in a fixed domain). *Find* $\{\hat{\mathbf{v}}_f, \hat{p}_f\} \in \{\hat{\mathbf{v}}_f^D + \hat{\mathbf{V}}_f^0\} \times \hat{\mathcal{L}}_f^0$ such that the initial data $\hat{\mathbf{v}}_f(0) = \hat{\mathbf{v}}_f^0$ are satisfied, and for almost all time steps $t \in I$ holds:

$$\begin{aligned}\hat{\rho}_f (\hat{J} \partial_t \hat{\mathbf{v}}_f, \hat{\boldsymbol{\psi}}^v)_{\widehat{\Omega}_f} + \hat{\rho}_f (\hat{J} \widehat{\mathbf{F}}^{-1} (\hat{\mathbf{v}}_f - \hat{\mathbf{w}}) \cdot \widehat{\nabla} \hat{\mathbf{v}}_f, \hat{\boldsymbol{\psi}}^v)_{\widehat{\Omega}_f} + (\hat{J} \widehat{\boldsymbol{\sigma}}_f \widehat{\mathbf{F}}^{-T}, \widehat{\nabla} \hat{\boldsymbol{\psi}}^v)_{\widehat{\Omega}_f} \\ - \langle \hat{J} \hat{\mathbf{g}}_f \widehat{\mathbf{F}}^{-T} \hat{\mathbf{n}}_f, \hat{\boldsymbol{\psi}}^v \rangle_{\widehat{\Gamma}_{f,N}} - \langle \hat{J} \widehat{\boldsymbol{\sigma}}_f \widehat{\mathbf{F}}^{-T} \hat{\mathbf{n}}_f, \hat{\boldsymbol{\psi}}^v \rangle_{\widehat{\Gamma}_i} - \hat{\rho}_f (\hat{J} \hat{\mathbf{f}}_f, \hat{\boldsymbol{\psi}}^v)_{\widehat{\Omega}_f} = 0, \\ (\widehat{\text{div}}(\hat{J} \widehat{\mathbf{F}}^{-1} \hat{\mathbf{v}}_f, \hat{\boldsymbol{\psi}}^p)_{\widehat{\Omega}_f} = 0,\end{aligned}$$

for all $\hat{\boldsymbol{\psi}}^v \in \hat{\mathcal{V}}_f^0$ and $\hat{\boldsymbol{\psi}}^p \in \hat{\mathcal{L}}_f^0$, and with the transformed Cauchy stress tensor:

$$\hat{\boldsymbol{\sigma}}_f = -\hat{p}_f \hat{\mathbf{I}} + 2\hat{\rho}_f \nu_f \hat{\mathbf{D}}(\hat{\mathbf{v}}_f) = -\hat{p}_f \hat{\mathbf{I}} + 2\hat{\rho}_f \nu_f (\hat{\nabla} \hat{\mathbf{v}}_f \hat{\mathbf{F}}^{-1} + \hat{\mathbf{F}}^{-T} \hat{\nabla} \hat{\mathbf{v}}_f^T), \quad (1)$$

Neumann data are denoted by $\hat{\mathbf{g}}_f$. For instance, a correction term for the do-nothing (see [45]) outflow condition has Neumann character:

$$\hat{\mathbf{g}}_f = -\hat{\rho}_f \nu_f \hat{\mathbf{F}}^{-T} \hat{\nabla} \hat{\mathbf{v}}_f^T \quad \text{on } \hat{\Gamma}_{f,N} = \hat{\Gamma}_{\text{out}}. \quad (2)$$

Remark 2.1. Coupling fluid flows with structural deformations along an interface $\hat{\Gamma}_i$ requires the fulfillment of two coupling conditions. Fluid flows need a Dirichlet condition on $\hat{\Gamma}_i$, i.e., the continuity of the velocities is strongly enforced in the corresponding Sobolev spaces. The structure problem is driven from the normal stresses that act on $\hat{\Gamma}_i$ and which are caused by the fluid. These normal stresses are achieved with the help of the term boundary term:

$$\langle \hat{J} \hat{\boldsymbol{\sigma}}_f \hat{\mathbf{F}}^{-T} \hat{\mathbf{n}}_f, \hat{\boldsymbol{\psi}}^v \rangle_{\hat{\Gamma}_i} \quad \text{on } \hat{\Gamma}_i.$$

The equations for structures are already defined in a Lagrangian sense, therefore, in a fixed domain $\hat{\Omega}_s$. Consequently, there is no additional effort to define them in the ALE framework. The boundary of $\hat{\Omega}_s$ is again split into the three types of boundaries as already discussed before. The sought physical unknowns are the vector-valued displacement $\hat{\mathbf{u}}_s$, the vector-valued velocity $\hat{\mathbf{v}}_s$.

Considerations on the damped wave equation

We make a side trip to briefly formulate our approach to circumvent the difficulties on the outflow boundary. In the last years, a lot of effort has been spent in modeling appropriate boundary conditions for the fluid and pressure for the inlet and outlet boundaries [1, 5, 6, 28, 29]; and many references cited therein. To overcome this deficiency, we prolongate the computational domain. Second, it is not clear which boundary conditions should be imposed for the structure on the outlet part. In the artificial extension of the computational domain, though, we use a damped version of the structure equations, to absorb incoming waves preventing reflections [7, 8]. This approach is well-known (for example, in acoustics) as *perfectly matched layer* (PML) layer [27]. We utilize the PML layer for fluid-structure interaction simulations, which is a novel aspect.

In the following, we introduce linear damping terms for the hyperbolic structure equations. For *strong* damping, we use the linearized Green-Lagrange strain tensor

$$\hat{\mathbf{E}}(\hat{\mathbf{u}}_s) \approx \hat{\boldsymbol{\epsilon}}(\hat{\mathbf{u}}_s) = \frac{1}{2} (\hat{\nabla} \hat{\mathbf{u}}_s + \hat{\nabla} \hat{\mathbf{u}}_s^T).$$

Then, the modified equation in $\widehat{\Omega}_s^{\text{ext}}$ is defined as

$$\widehat{\rho}_s \partial_t^2 \widehat{u}_s - \widehat{\mathbf{div}}(\widehat{F}_s \widehat{\Sigma}) + \gamma_w \partial_t \widehat{u}_s - \gamma_s \partial_t \widehat{\mathbf{div}}(\widehat{\epsilon}(\widehat{u}_s)) = 0,$$

with $\gamma_s, \gamma_w \geq 0$. The first damping term is referred to as ‘weak damping’ whereas the second damping type is known as ‘strong damping’ because the full operator is used for the damping.

In the following, we pose a standard mixed formulation of the structure equations in $\widehat{\Omega}_s^{\text{ext}}$:

$$\begin{aligned} \widehat{\rho}_s \partial_t \widehat{v}_s - \widehat{\mathbf{div}}(\widehat{F}_s \widehat{\Sigma}) + \gamma_w \widehat{v}_s - \gamma_s \widehat{\mathbf{div}}(\widehat{\epsilon}(\widehat{v}_s)) &= 0, \\ \widehat{\rho}_s (\partial_t \widehat{u}_s - \widehat{v}_s) &= 0, \end{aligned} \quad (3)$$

Remark 2.2. The modified structure Problem 3 reduces to the undamped hyperbolic structure equations by setting the damping parameters to $\gamma_w = \gamma_s = 0$. Therefore, we are dealing in the following only with Problem 3 in $\widehat{\Omega}_s$.

As for fluid flows, let \widehat{v}_s^D and \widehat{u}_s^D be suitable extensions of Dirichlet inflow data. We use the mixed formulation (3), to obtain the formulation of the structure equations:

Problem 2.2 (Compressible structure problem). *Find*

$\{\widehat{v}_s, \widehat{u}_s\} \in \widehat{\mathcal{L}}_s \times \{\widehat{u}_s^D + \widehat{\mathcal{V}}_s^0\}$, such that $\widehat{v}_s(0) = \widehat{v}_s^0$ and $\widehat{u}_s(0) = \widehat{u}_s^0$ are satisfied, and for almost all time steps $t \in I$ holds:

$$\begin{aligned} (\widehat{\rho}_s \partial_t \widehat{v}_s, \widehat{\psi}^v)_{\widehat{\Omega}_s} + (\widehat{F} \widehat{\Sigma}, \widehat{\nabla} \widehat{\psi}^v)_{\widehat{\Omega}_s} - \langle \widehat{F} \widehat{\Sigma} \widehat{n}_s, \widehat{\psi}^v \rangle_{\widehat{\Gamma}_i \cup \widehat{\Gamma}_N} \\ + \gamma_w (\widehat{v}_s, \widehat{\psi}^v)_{\widehat{\Omega}_s} + \gamma_s (\widehat{\epsilon}(\widehat{v}_s), \widehat{\nabla} \widehat{\psi}^v)_{\widehat{\Omega}_s} \\ - \gamma_s \langle \widehat{\epsilon}(\widehat{v}_s) \widehat{n}_s, \widehat{\psi}^v \rangle_{\widehat{\Gamma}_i \cup \widehat{\Gamma}_N} - (\widehat{\rho}_s \widehat{f}_s, \widehat{\psi}^v)_{\widehat{\Omega}_s} = 0 \quad \forall \widehat{\psi}^v \in \widehat{\mathcal{V}}_s^0, \\ \widehat{\rho}_s (\partial_t \widehat{u}_s - \widehat{v}_s, \widehat{\psi}^u)_{\widehat{\Omega}_s} = 0 \quad \forall \widehat{\psi}^u \in \widehat{\mathcal{L}}_s, \end{aligned}$$

The constitutive stress tensor (namely the 2nd Piola-Kirchhoff tensor) is given by:

$$\widehat{F} \widehat{\Sigma} := \widehat{F} (\lambda_s (\text{tr} \widehat{E}) \widehat{I} + 2\mu_s \widehat{E}), \quad \widehat{E} = \frac{1}{2} (\widehat{F}^T \widehat{F} - \widehat{I}), \quad (4)$$

with the Lamé coefficients λ_s and μ_s . For the STVK material, the compressibility is related to the Poisson ratio ν_s ($\nu_s < \frac{1}{2}$).

2.3. Definition of the ALE mapping and geometrical coupling

The fluid mesh motion is reconstructed using an additional equation that is driven by the motion of the interface $\Gamma_i(t)$, i.e., $\hat{\mathcal{A}} = \hat{\mathbf{u}}_s$ on $\widehat{\Gamma}_i$, leading to $\hat{\mathbf{w}} = \hat{\mathbf{v}}_s$ on $\widehat{\Gamma}_i$. Furthermore, we fix the inlet and outlet boundary parts with $\hat{\mathbf{u}}_f = 0$ on $\widehat{\Gamma}_{f,\text{inlet}} \cup \widehat{\Gamma}_{f,\text{outlet}}$ (see Fig. 1 where $\widehat{\Gamma}_{f,\text{inlet}} = H$ and $\widehat{\Gamma}_{f,\text{outlet}} = D$). In the fluid domain $\widehat{\Omega}_f$ the transformation $\hat{\mathcal{A}}$ is arbitrary but should satisfy certain regularity conditions (C^1 -diffeomorphism) [5]. In this study, the fluid mesh movement is constructed by solving an harmonic problem (for stationary configurations) or a biharmonic equation (for large mesh deformations without remeshing). We solve:

$$\begin{cases} \Delta \hat{\mathbf{u}}_f = 0 & \text{in } \widehat{\Omega}_f & \text{(harmonic),} \\ \Delta^2 \hat{\mathbf{u}}_f = 0 & \text{in } \widehat{\Omega}_f & \text{(biharmonic),} \\ \hat{\mathbf{u}}_f = 0 & \text{on } \widehat{\Gamma}_{f,\text{inlet}} \cup \widehat{\Gamma}_{f,\text{outlet}} & \text{(harmonic),} \\ \hat{\mathbf{u}}_f = \partial_n \hat{\mathbf{u}} = 0 & \text{on } \widehat{\Gamma}_{f,\text{inlet}} \cup \widehat{\Gamma}_{f,\text{outlet}} & \text{(biharmonic),} \\ \hat{\mathbf{u}}_f = \hat{\mathbf{u}}_s & \text{on } \widehat{\Gamma}_i & \text{(harmonic),} \\ \hat{\mathbf{u}}_f = \hat{\mathbf{u}}_s \quad \text{and} \quad \partial_n \hat{\mathbf{u}}_f = \partial_n \hat{\mathbf{u}}_s & \text{on } \widehat{\Gamma}_i & \text{(biharmonic).} \end{cases}$$

On the remaining boundary parts $\widehat{\Gamma}_{\text{wall}}$, we prescribe no Dirichlet conditions such that the structure is allowed to move. In a fully coupled variational formulation, these equations are used within a weak formulation. Thus, we define

$$\widehat{\boldsymbol{\sigma}}_{\text{mesh}} := \alpha \widehat{\nabla} \hat{\mathbf{u}}_f, \quad (5)$$

where $\alpha > 0$ can be chosen accordingly to [30-32].

2.4. The monolithic formulation of the coupled problem

The monolithic setting of the coupled equations of Problem 2.1 with 2.2 is derived in the same manner as [8, 32], and the many references cited therein. Using this approach, all equations are defined (and solved) in the reference configuration $\widehat{\Omega} = \widehat{\Omega}_f \cup \widehat{\Omega}_s$.

Continuity of velocity and stress

The velocity field must be continuous on the interface (which is a Dirichlet-like condition seen from the fluid side). A priori, we assume sufficient regularity for the structure velocity such that it can be given to the fluid problem. In detail, we have

$$\mathbf{v}_f = \mathbf{w} = \mathbf{v}_s \quad \text{on } \Gamma_i. \quad (6)$$

To complete the structure equations, we must enforce the balance of the normal stresses on the interface:

$$\hat{J}\hat{\sigma}_f\hat{F}^{-T}\hat{n}_f + \hat{F}\hat{\Sigma}\hat{n}_s + \gamma_s\hat{\epsilon}(\hat{v}_s)\hat{n}_s = 0 \quad \text{on } \hat{\Gamma}_i. \quad (7)$$

This condition corresponds to a Neumann-like boundary condition for the structure subsystem. We point out, that an additional term $\gamma_s\hat{\epsilon}(\hat{v}_s)\hat{n}_s$ must be considered when we work with strong structural damping.

Then, the weak form reads:

Problem 2.3 (Practicable FSI with harmonic mesh motion). *Find* $\{\hat{v}_f, \hat{v}_s, \hat{u}_f, \hat{u}_s, \hat{p}_f\} \in \{\hat{v}_f^D + \hat{V}_{f,\hat{v}}^0\} \times \hat{\mathcal{L}}_s \times \{\hat{u}_f^D + \hat{V}_{f,\hat{u}}^0\} \times \{\hat{u}_s^D + \hat{V}_s^0\} \times \hat{\mathcal{L}}_f^0$, such that $\hat{v}_f(0) = \hat{v}_f^0$, $\hat{v}_s(0) = \hat{v}_s^0$, $\hat{u}_f(0) = \hat{u}_f^0$, and $\hat{u}_s(0) = \hat{u}_s^0$ are satisfied, and for almost all time steps $t \in I$ holds:

$$\begin{aligned} & (\hat{J}\hat{\rho}_f\partial_t\hat{v}_f, \hat{\psi}^v)_{\hat{\Omega}_f} + (\hat{\rho}_f\hat{J}(\hat{F}^{-1}(\hat{v}_f - \hat{w}) \cdot \hat{\nabla})\hat{v}_f, \hat{\psi}^v)_{\hat{\Omega}_f} \\ & + (\hat{J}\hat{\sigma}_f\hat{F}^{-T}, \hat{\nabla}\hat{\psi}^v)_{\hat{\Omega}_f} - \langle \hat{g}, \hat{\psi}^v \rangle_{\hat{\Gamma}_N} - (\hat{\rho}_f\hat{J}\hat{f}_f, \hat{\psi}^v)_{\hat{\Omega}_f} = 0 \quad \forall \hat{\psi}^v \in \hat{V}_{f,\hat{\Gamma}_i}^0, \\ & \quad (\hat{\rho}_s\partial_t\hat{v}_s, \hat{\psi}^v)_{\hat{\Omega}_s} + (\hat{F}\hat{\Sigma}, \hat{\nabla}\hat{\psi}^v)_{\hat{\Omega}_s} \\ & + \gamma_w(\hat{v}_s, \hat{\psi}^v)_{\hat{\Omega}_s} + \gamma_s(\hat{\epsilon}(\hat{v}_s), \hat{\nabla}\hat{\psi}^v)_{\hat{\Omega}_s} - (\hat{\rho}_s\hat{f}_s, \hat{\psi}^v)_{\hat{\Omega}_s} = 0 \quad \forall \hat{\psi}^v \in \hat{V}_s^0, \\ & \quad (\hat{\sigma}_{mesh}, \hat{\nabla}\hat{\psi}^u)_{\hat{\Omega}_f} = 0 \quad \forall \hat{\psi}^u \in \hat{V}_{f,\hat{u},\hat{\Gamma}_i}^0, \\ & \quad \hat{\rho}_s(\partial_t\hat{u}_s - \hat{v}_s, \hat{\psi}^u)_{\hat{\Omega}_s} = 0 \quad \forall \hat{\psi}^u \in \hat{\mathcal{L}}_s \\ & \quad (\widehat{\text{div}}(\hat{J}\hat{F}^{-1}\hat{v}_f), \hat{\psi}^p)_{\hat{\Omega}_f} = 0 \quad \forall \hat{\psi}^p \in \hat{\mathcal{L}}_f^0, \end{aligned}$$

with $\hat{\rho}_f$, $\hat{\rho}_s$, ν_f , μ_s , λ_s , \hat{F} , and \hat{J} as defined before. The stress tensors $\hat{\sigma}_f$, $\hat{\Sigma}$, and $\hat{\sigma}_{mesh}$ are defined in the Equations (1), (4), and in (5).

To solve the nonlinear problem, we introduce a semi-linear form and write the problem in compact notation.

In the domain $\hat{\Omega}$ and the time interval $I = [0, T]$, we consider the fluid-structure interaction Problem 2.3 with harmonic or linear-elastic mesh motion in an abstract setting (the biharmonic problem is straightforward): Find $\hat{U} = \{\hat{v}_f, \hat{v}_s, \hat{u}_f, \hat{u}_s, \hat{p}_f\} \in \hat{X}_D^0$, where $\hat{X}_D^0 := \{\hat{v}_f^D + \hat{V}_{f,\hat{v}}^0\} \times \hat{\mathcal{L}}_s \times \{\hat{u}_f^D + \hat{V}_{f,\hat{u}}^0\} \times \{\hat{u}_s^D + \hat{V}_s^0\} \times \hat{\mathcal{L}}_f^0$, such that

$$\int_0^T \hat{A}(\hat{U})(\hat{\Psi}) dt = \int_0^T \hat{F}(\hat{\Psi}) dt \quad \forall \hat{\Psi} \in \hat{X}, \quad (8)$$

where $\hat{\Psi} = \{\hat{\psi}_f^v, \hat{\psi}_s^v, \hat{\psi}_f^u, \hat{\psi}_s^u, \hat{\psi}_f^p\}$ and $\hat{X} = \hat{V}_{f,\hat{v}}^0 \times \hat{\mathcal{L}}_s \times \hat{V}_{f,\hat{u},\hat{\Gamma}_i}^0 \times \hat{V}_s^0 \times \hat{\mathcal{L}}_f^0$. The time integral is defined in an abstract sense such that the equation holds for almost all time steps.

Problem 2.4 (Semi-linear form of FSI with harmonic mesh motion). *Using the harmonic mesh motion model leads to the following expressions of $\widehat{\mathbf{A}}(\widehat{\mathbf{U}})(\widehat{\Psi})$ and $\widehat{\mathbf{F}}(\widehat{\Psi})$:*

$$\widehat{\mathbf{F}}(\widehat{\Psi}) = (\widehat{\rho}_s \widehat{\mathbf{f}}_s, \widehat{\psi}^v)_{\widehat{\Omega}_s}, \quad (9)$$

and

$$\begin{aligned} \widehat{\mathbf{A}}(\widehat{\mathbf{U}})(\widehat{\Psi}) &= (\widehat{J} \widehat{\rho}_f \partial_t \widehat{\mathbf{v}}_f, \widehat{\psi}_f^v)_{\widehat{\Omega}_f} + (\widehat{\rho}_f \widehat{J} (\widehat{\mathbf{F}}^{-1} \widehat{\mathbf{v}}_f \cdot \widehat{\nabla}) \widehat{\mathbf{v}}_f, \widehat{\psi}_f^v)_{\widehat{\Omega}_f} \\ &\quad - (\widehat{\rho}_f \widehat{J} (\widehat{\mathbf{F}}^{-1} \widehat{\mathbf{w}} \cdot \widehat{\nabla}) \widehat{\mathbf{v}}_f, \widehat{\psi}_f^v)_{\widehat{\Omega}_f} - \langle \widehat{\mathbf{g}}_f, \widehat{\psi}_f^v \rangle_{\widehat{\Gamma}_N} - (\widehat{\rho}_f \widehat{J} \widehat{\mathbf{f}}_f, \widehat{\psi}_f^v)_{\widehat{\Omega}_f} \\ &\quad + (\widehat{J} \widehat{\sigma}_f \widehat{\mathbf{F}}^{-T}, \widehat{\nabla} \widehat{\psi}_f^v)_{\widehat{\Omega}_f} + (\widehat{\rho}_s \partial_t \widehat{\mathbf{v}}_s, \widehat{\psi}_s^v)_{\widehat{\Omega}_s} + (\widehat{\mathbf{F}} \widehat{\Sigma}, \widehat{\nabla} \widehat{\psi}_s^v)_{\widehat{\Omega}_s} \\ &\quad + (\widehat{\rho}_s \partial_t \widehat{\mathbf{u}}_s, \widehat{\psi}_s^u)_{\widehat{\Omega}_s} - (\widehat{\rho}_s \widehat{\mathbf{v}}_s, \widehat{\psi}_s^u)_{\widehat{\Omega}_s} + (\alpha_u \widehat{\nabla} \widehat{\mathbf{u}}_f, \widehat{\nabla} \widehat{\psi}_f^u)_{\widehat{\Omega}_f} \\ &\quad + \gamma_w (\widehat{\mathbf{v}}_s, \widehat{\psi}_s^v)_{\widehat{\Omega}_s} + \gamma_s (\widehat{\epsilon}(\widehat{\mathbf{v}}_s), \widehat{\nabla} \widehat{\psi}_s^v)_{\widehat{\Omega}_s}, \\ &\quad + (\widehat{\text{div}}(\widehat{J} \widehat{\mathbf{F}}^{-1} \widehat{\mathbf{v}}_f), \widehat{\psi}_f^p)_{\widehat{\Omega}_f}. \end{aligned} \quad (10)$$

3. Discretization and Adaptive Mesh Refinement

For temporal integration of Equation (8), we use the shifted Crank-Nicolson scheme based on finite differences that was developed for our ALE scheme in a prior work [32]. Spatial discretization in the reference configuration $\widehat{\Omega}$ is treated with a conforming Galerkin finite element scheme, leading to a finite dimensional subspace $\widehat{\mathbf{X}}_h \subset \widehat{\mathbf{X}}$. The discrete spaces are based on the Q_2^c/P_1^{dc} element for the fluid problem. The structure problem is discretized with the Q_2^c element. The nonlinear problem is solved with the Newton method where the Jacobian is derived by exact linearization of the directional derivatives [8].

Modeling blood flow at the exit of the aortic valve leads to a convection dominated problem with a Reynolds number ~ 4500 [22]. For this reason, we need to stabilize our formulation. Residual based stabilization was first introduced in [33] and was intensively analyzed [34]. Our method of choice is a rough simplification of the streamline upwind Petrov-Galerkin (SUPG) method. This term in the reference configuration $\widehat{\Omega}_f$ on each cell $\widehat{K} \in \mathcal{T}_h$ reads

$$\widehat{\mathbf{S}}_{\text{stab}}(\widehat{\mathbf{U}}_h^n)(\widehat{\Psi}) := \sum_{\widehat{K} \in \mathcal{T}_h} (\widehat{\rho}_f (\widehat{J} \widehat{\mathbf{F}}^{-1} \widehat{\mathbf{v}}_f \cdot \widehat{\nabla}) \widehat{\mathbf{v}}_f, \delta_{K,n} (\widehat{\mathbf{F}}^{-1} \widehat{\mathbf{v}}_f \cdot \widehat{\nabla}) \widehat{\psi}_f^v)_{\widehat{K}}. \quad (11)$$

with

$$\delta_{K,m} = \delta_0 \frac{h_K^2}{6\nu_f + h_K \|\mathbf{v}_{kh}\|_K}, \quad \delta_0 = 0.1.$$

For more details on the choice of these parameters, we refer to [35].

3.1. Adaptive Mesh Refinement

This *core* chapter is devoted to efficient mesh refinement techniques for solving fluid-structure interaction problems. The main goal is to derive a posteriori error estimates that accounts for the error between the continuous solution and the discrete solution with respect to a given quantity of interest (such as point deflections or the measurement of wall stresses). This a posteriori error estimate is used for the mesh adaptation of (stationary) fluid-structure interaction problems. The adaptive solution is derived by employing the *dual weighted residual method* (DWR) method. This method was systematically developed in [16] and requires a common, i.e., monolithic, variational formulation of the coupled problem as introduced before. In the last years, the DWR method for spatial refinement has been successfully applied to different kind of applications. The extension to a fully space-time DWR approach was made in [36, 37]. Specifically, DWR approaches (for spatial refinement) for fluid-structure interaction problems are investigated by others [17, 19-21]. In contrast to most of the other works, e.g., [19], we use in this study the strong residual for the error estimator as originally suggested in [38].

The main motivation for such developments is, that error measurements in global norms does not provide useful error bounds for the error of the quantity of interest. Thus, the new aspect in this work (compared to the previously cited work) is the application of a simplified version of the DWR method to stationary valve simulations [39]. Indeed, the validation of the DWR method for valve settings and the choice of wall stress measurement as goal functional has important consequences for the numerical solution of such problems. First, the wall stress measurement is important for clinical applications and (possible) comparisons with clinical data. Second, realistic valve simulations must be done in three dimensions for which global mesh refinement becomes prohibitive. Thus, the prototypical investigations of this chapter are the basis for future development.

We use:

- Global mesh refinement;
- Smoothness-based mesh refinement;
- Goal-oriented mesh refinement with the DWR method.

The first procedure is self-explaining and the other two techniques are discussed in the following.

Smoothness-based mesh refinement

One possibility to obtain refinement indicators that drive a mesh adaption procedure is based on measuring the jumps of the cell edges of the computed discrete solution \hat{U}_h . The local error indicators that are used to adapt the mesh read

$$\eta_{\hat{K}}^2 = \hat{h} \int_{\hat{K}} [\partial_n \hat{U}_h]^2 d\hat{s}, \quad (12)$$

and where $[\cdot]$ denotes the jump across inter-cell boundaries. The mesh is adapted in those regions, where we evaluate the largest jumps. This heuristic procedure is often used for mesh adaption in the literature and it was suggested in [40, 41]. However, all local error indicators have the same influence on the total error and therefore, on the mesh refinement. For instance, the discrete solution \hat{U}_h consists of the contributions

$$\hat{v}_{f,h}, \hat{v}_{s,h}, \hat{u}_{f,h}, \hat{u}_{s,h}, \hat{p}_{f,h}.$$

With appropriate weighting of the single solutions, one can influence the behavior of this estimator dramatically. How to weight the local error contributions appropriately solving an adjoint problem is subject of the discussion in the following.

3.2. Goal oriented mesh adaption with the DWR method

The Galerkin approximation to Equation (8) (neglecting the time derivatives and stabilization terms), reads: Find $\hat{U}_h = \{\hat{v}_{f,h}, \hat{v}_{s,h}, \hat{u}_{f,h}, \hat{u}_{s,h}, \hat{p}_{f,h}\} \in \hat{X}_{h,D}^0$, where $\hat{X}_{h,D}^0 := \{\hat{v}_{f,h}^D + \hat{V}_{f,\hat{v},h}^0\} \times \hat{L}_{s,h} \times \{\hat{u}_{f,h}^D + \hat{V}_{f,\hat{u},h}^0\} \times \{\hat{u}_{s,h}^D + \hat{V}_{s,h}^0\} \times \hat{L}_{f,h}^0$, such that

$$\hat{A}(\hat{U}_h)(\hat{\Psi}_h) = \hat{F}(\hat{\Psi}_h) \quad \forall \hat{\Psi}_h \in \hat{X}_h. \quad (13)$$

The solution \hat{U}_h is used to calculate an approximation $J(\hat{U}_h)$ of the goal-functional $J(\hat{U}) : \hat{X} \rightarrow \mathbb{R}$. This functional is assumed to be sufficiently differentiable. Concretely, it is used for the evaluation of point values (the deflection of the valve), line integrals (the computation of the stresses), or domain integrals (L^2 -norm of the velocity).

Example 3.1 *The error of a deflection \hat{u}_s in y-direction at some point $\hat{p} \in \widehat{\Omega}$*

can be estimated using the following (regularized) functional:

$$J(\hat{u}_{s,y}) := |B_\varepsilon|^{-1} \int_{B_\varepsilon} \hat{u}_{y,s} d\hat{x} = \hat{u}_{y,s}(\hat{p}) + O(\varepsilon^2),$$

where B_ε is the ε -ball around the point \hat{p} .

Example 3.2 *The error of mean normal fluxes over lower-dimensional manifolds. For example, we compute the error of wall stresses in y-direction along the interface between the fluid and the structure, which can be estimated with*

$$J(\hat{\mathbf{U}}) := \int_{\hat{S}} \hat{\mathbf{J}} \hat{\boldsymbol{\sigma}}_f \hat{\mathbf{F}}^{-T} \hat{\mathbf{n}}_f \hat{\mathbf{d}} d\hat{s},$$

where $\hat{\mathbf{d}}$ is a unit vector perpendicular to the mean flow direction. Later, we compute the wall stresses along the interface of the aorta $\hat{S} := \widehat{\Gamma}_{aorta}$. In particular, accurate wall stress measurement is important for clinical applications.

We use the (formal) Euler-Lagrange method, to derive a computable representation of the approximation error $J(\hat{\mathbf{U}}) - J(\hat{\mathbf{U}}_h)$. Concretely, the task is

$$\min\{J(\hat{\mathbf{U}}) - J(\hat{\mathbf{U}}_h)\} \quad \text{s.t.} \quad \hat{\mathbf{A}}(\hat{\mathbf{U}})(\hat{\boldsymbol{\Psi}}) = \hat{\mathbf{F}}(\hat{\boldsymbol{\Psi}}) \quad \forall \hat{\boldsymbol{\Psi}} \in \hat{\mathbf{X}}.$$

As usual for optimization problems, we introduce a dual variable $\hat{\mathbf{Z}}$ (usually referred to as *sensitivity*) to formulate the Lagrangian functional

$$\mathcal{L}(\hat{\mathbf{U}}, \hat{\mathbf{Z}}) = J(\hat{\mathbf{U}}) + \hat{\mathbf{F}}(\hat{\mathbf{Z}}) - \hat{\mathbf{A}}(\hat{\mathbf{U}})(\hat{\mathbf{Z}}).$$

We obtain the optimality system

$$\begin{aligned} \mathcal{L}'_{\hat{\mathbf{Z}}}(\hat{\mathbf{U}}, \hat{\mathbf{Z}})(\delta \hat{\mathbf{Z}}) &= \hat{\mathbf{F}}(\delta \hat{\mathbf{Z}}) - \hat{\mathbf{A}}(\hat{\mathbf{U}})(\delta \hat{\mathbf{Z}}) = 0 \quad \delta \hat{\mathbf{Z}} \in \hat{\mathbf{X}}, \\ \mathcal{L}'_{\hat{\mathbf{U}}}(\hat{\mathbf{U}}, \hat{\mathbf{Z}})(\delta \hat{\mathbf{U}}) &= J'(\hat{\mathbf{U}})(\delta \hat{\mathbf{U}}) - \hat{\mathbf{A}}'_{\hat{\mathbf{U}}}(\hat{\mathbf{U}})(\delta \hat{\mathbf{U}}, \hat{\mathbf{Z}}) = 0 \quad \delta \hat{\mathbf{U}} \in \hat{\mathbf{X}}. \end{aligned}$$

In this context, we deal with a *primal* problem and a *dual* problem. The primal problem corresponds to the original equation. In an appropriate discrete space $\hat{\mathbf{X}}_h \subset \hat{\mathbf{X}}$, the discrete problem reads:

$$\begin{aligned} \mathcal{L}'_{\hat{\mathbf{Z}}}(\hat{\mathbf{U}}_h, \hat{\mathbf{Z}}_h)(\delta \hat{\mathbf{Z}}_h) &= \hat{\mathbf{F}}(\hat{\mathbf{Z}}_h) - \hat{\mathbf{A}}(\hat{\mathbf{U}}_h)(\delta \hat{\mathbf{Z}}_h) = 0 \quad \delta \hat{\mathbf{Z}}_h \in \hat{\mathbf{X}}_h, \\ \mathcal{L}'_{\hat{\mathbf{U}}}(\hat{\mathbf{U}}_h, \hat{\mathbf{Z}}_h)(\delta \hat{\mathbf{U}}_h) &= J'(\hat{\mathbf{U}}_h)(\delta \hat{\mathbf{U}}_h) - \hat{\mathbf{A}}'_{\hat{\mathbf{U}}}(\hat{\mathbf{U}}_h)(\delta \hat{\mathbf{U}}_h, \hat{\mathbf{Z}}_h) = 0 \quad \delta \hat{\mathbf{U}}_h \in \hat{\mathbf{X}}_h. \end{aligned} \quad (14)$$

For given solutions $\{\hat{\mathbf{U}}, \hat{\mathbf{Z}}\}$ and $\{\hat{\mathbf{U}}_h, \hat{\mathbf{Z}}_h\}$ we obtain the following identity for the approximation error:

$$J(\hat{\mathbf{U}}) - J(\hat{\mathbf{U}}_h) = \mathcal{L}(\hat{\mathbf{U}}, \hat{\mathbf{Z}}) - \mathcal{L}(\hat{\mathbf{U}}_h, \hat{\mathbf{Z}}_h).$$

To *compute* this relation, we use the results of [16] and we obtain:

Theorem 3.3 *For any solution of the Problem 13, we obtain the error representation*

$$J(\hat{\mathbf{U}}) - J(\hat{\mathbf{U}}_h) = \frac{1}{2} \rho(\hat{\mathbf{U}}_h)(\hat{\mathbf{Z}} - \hat{\boldsymbol{\Psi}}_h) + \frac{1}{2} \rho^*(\hat{\mathbf{U}}_h, \hat{\mathbf{Z}}_h)(\hat{\mathbf{U}} - \hat{\boldsymbol{\Phi}}_h) + \mathcal{R}_h^{(3)}, \quad (15)$$

for all $\{\hat{\Phi}_h, \hat{\Psi}_h\} \in \hat{X}_h \times \hat{X}_h$ and with the primal and dual residuals:

$$\begin{aligned} \rho(\hat{U}_h)(\hat{Z} - \hat{\Psi}_h) &:= -A(\hat{U}_h)(\cdot), \\ \rho^*(\hat{U}_h, \hat{Z}_h)(\hat{U} - \hat{\Phi}_h) &:= J'(\hat{U}_h)(\cdot) - A'(\hat{U}_h)(\cdot, \hat{Z}_h). \end{aligned}$$

The remainder term is $\mathcal{R}_h^{(3)}$ is cubic in the primal and the dual errors. This error identity can be used to drive an automatic mesh refinement process and/or can be adopted to estimate the error.

Proof. We refer to [16] for a proof of this theorem. \square

The dual variable $\hat{Z} = \{\hat{z}_f^v, \hat{z}_s^v, \hat{z}_f^u, \hat{z}_s^u, \hat{z}_f^p\}$ is computed with the corresponding (linearized) dual problem (obtained as first equation in (14))

$$A'(\hat{U}_h)(\hat{\Psi}_h, \hat{Z}_h) = J'(\hat{\Psi}_h), \quad \forall \hat{\Psi}_h \in \tilde{X}_h, \quad (16)$$

where not necessarily $\tilde{X}_h = \hat{X}_h$. The matrix \hat{A}' denotes the transposed matrix

of the primal problem and it is assembled as one further Newton Jacobian in the nonlinear solution process; we refer to [42]. The dual Problem (16) can be solved with a global higher approximation or local higher interpolation. With these solutions, we obtain approximations of the differences $\hat{Z} - \hat{\Psi}_h$ in the error representation (15). The solvability of the primal problem and the dual problem is not for granted, we refer for a deeper discussion to [18].

To obtain a *computable* version of the error identity, we set up some assumptions. First, we neglect the remainder term $\mathcal{R}_h^{(3)}$. Second, we only use the primal residual $\rho(\hat{U}_h)(\hat{Z} - \hat{\Psi}_h)$ to estimate the error (a discussion on this topic can be found in [42]). Third, we transform (as originally suggested in [38]) the error identity with cell-wise partial integration into the strong form, leading to a challenging form of the Laplacian term of the transformed fluid equations. Because we are only dealing with moderate deformations, we assume (while computing the error) that $\hat{F} = \hat{I}$ and $\hat{J} = 1$, and a symmetric stress tensor:

$$(\hat{J}\hat{\sigma}_{f,vu}\hat{F}^{-T}, \hat{\nabla}\hat{\psi}^v)_{\hat{\Omega}_f}, \quad \hat{\sigma}_{f,vu} := \hat{\rho}_f\nu_f(\hat{\nabla}\hat{v}_f\hat{F}^{-1} + \hat{F}^{-T}\hat{\nabla}\hat{v}_f^T),$$

leading to

$$(\hat{\sigma}_{appr}, \hat{\nabla}\hat{\psi}^v)_{\hat{\Omega}_f}, \quad \hat{\sigma}_{appr} := \hat{\rho}_f\nu_f(\hat{\nabla}\hat{v}_f + \hat{\nabla}\hat{v}_f^T).$$

This can be easily transformed into the strong formulation. Basically the same idea is used for the constitutive tensor of the structure (here the STVK material):

$$(\hat{F}\hat{\Sigma}, \hat{\nabla}\hat{\psi}^v)_{\hat{\Omega}_s}, \quad \hat{\Sigma} := (\lambda_s(\text{tr}\hat{E})\hat{I} + 2\mu_s\hat{E}).$$

Consequently, the structure tensor is approximated as

$$\begin{aligned}
 \widehat{\Sigma}_{\text{appr}} &:= (\lambda_s(\text{tr}\widehat{\mathbf{E}})\widehat{\mathbf{I}} + 2\mu_s\widehat{\mathbf{E}}) \\
 &\approx \lambda_s\text{div}(\widehat{\mathbf{u}}_s)\widehat{\mathbf{I}} + 2\mu_s\frac{1}{2}(\widehat{\nabla}\widehat{\mathbf{u}}_s + \widehat{\nabla}\widehat{\mathbf{u}}_s^T) \\
 &= \lambda_s\text{div}(\widehat{\mathbf{u}}_s)\widehat{\mathbf{I}} + (\mu_s\widehat{\nabla}\widehat{\mathbf{u}}_s + \widehat{\nabla}\widehat{\mathbf{u}}_s^T).
 \end{aligned}$$

Finally, we notice that the structure damping terms vanish in a fully stationary setting. This is due to the fact that the structure velocity equals zero but however, it is used for structural damping. Consequently, the damping terms are equal to zero, too.

Hence, we obtain the following error representation:

Proposition 3.4 *With the previous assumptions, we have for stationary fluid-structure interaction the error representation*

$$J(\widehat{\mathbf{U}}) - J(\widehat{\mathbf{U}}_h) \approx \eta_h^f + \eta_h^s + \eta_h^i,$$

where we split the local error indicators into fluid η_h^f , structure η_h^s , and interface contributions η_h^i . In detail, we have

$$\begin{aligned}
 \eta_h^f &:= \sum_{\widehat{K} \in \widehat{\mathcal{T}}_h} \{ (-\widehat{\rho}_f \widehat{J}(\widehat{\mathbf{F}}^{-1} \widehat{\mathbf{v}}_f \cdot \widehat{\nabla}) \widehat{\mathbf{v}}_f + \widehat{\nabla} \cdot \widehat{\sigma}_{\text{appr}} - \widehat{\nabla} \widehat{\rho}_f, \widehat{\mathbf{z}}_f^v - \widehat{\psi}_h^v)_{\widehat{K}_f} \\
 &\quad + \frac{1}{2} ([\widehat{J} \widehat{\sigma}_f \widehat{\mathbf{F}}^{-T} \widehat{\mathbf{n}}_f], \widehat{\mathbf{z}}_f^v - \widehat{\psi}_h^v)_{\partial \widehat{K}_f \setminus \partial \widehat{\Omega} \cup \widehat{\Gamma}_i} + (\widehat{\text{div}}(\widehat{J} \widehat{\mathbf{F}}^{-1} \widehat{\mathbf{v}}_f), \widehat{\mathbf{z}}_f^p - \widehat{\psi}_h^p)_{\widehat{K}_f} \\
 &\quad + (\widehat{\nabla} \cdot \widehat{\sigma}_{\text{mesh}}, \widehat{\mathbf{z}}_f^u - \widehat{\psi}_h^u)_{\widehat{K}_f} + \frac{1}{2} ([\widehat{\sigma}_{\text{mesh}} \widehat{\mathbf{n}}_f], \widehat{\mathbf{z}}_f^u - \widehat{\psi}_h^u)_{\partial \widehat{K}_f \setminus \partial \widehat{\Omega} \cup \widehat{\Gamma}_i} \}
 \end{aligned}$$

and

$$\eta_h^s := \sum_{\widehat{K} \in \widehat{\mathcal{T}}_h} \{ (\widehat{\nabla} \cdot \widehat{\Sigma}_{\text{appr}}, \widehat{\mathbf{z}}_s^v - \widehat{\psi}_h^v)_{\widehat{K}_s} + \frac{1}{2} ([\widehat{\mathbf{F}} \widehat{\Sigma}_{\text{appr}} \widehat{\mathbf{n}}_s], \widehat{\mathbf{z}}_s^v - \widehat{\psi}_h^v)_{\partial \widehat{K}_s \setminus \partial \widehat{\Omega} \cup \widehat{\Gamma}_i} \},$$

and

$$\begin{aligned}
 \eta_h^i &:= \sum_{\widehat{K} \in \widehat{\mathcal{T}}_h} \{ \frac{1}{2} ([\widehat{J} \widehat{\sigma}_f \widehat{\mathbf{F}}^{-T} \widehat{\mathbf{n}}_f], \widehat{\mathbf{z}}_f^v - \widehat{\psi}_h^v)_{\widehat{\Gamma}_i} + \frac{1}{2} ([\widehat{\sigma}_{\text{mesh}} \widehat{\mathbf{n}}_f], \widehat{\mathbf{z}}_f^u - \widehat{\psi}_h^u)_{\widehat{\Gamma}_i} \\
 &\quad + \frac{1}{2} ([\widehat{\mathbf{F}} \widehat{\Sigma}_{\text{appr}} \widehat{\mathbf{n}}_s], \widehat{\mathbf{z}}_s^v - \widehat{\psi}_h^v)_{\widehat{\Gamma}_i} \},
 \end{aligned}$$

where $\widehat{\sigma}_{\text{mesh}}$ was defined in Section 2.3 and where $[\cdot]$ denotes the jump across inter-cell boundaries.

The previous declared error representation consists of the *cell residuals* (measuring the consistency of the discrete solution $\hat{\mathbf{U}}_h$) and the edge terms $[\cdot]$ (measuring the discrete smoothness). The latter one has similar properties to the smoothness-based refinement indicators as introduced before. The residuals terms are weighted with so-called *sensitivity factors*

$$\hat{\mathbf{z}}_{f,s}^v - \hat{\boldsymbol{\psi}}_h^v, \quad \hat{\mathbf{z}}_{f,s}^u - \hat{\boldsymbol{\psi}}_h^u, \quad \hat{\mathbf{z}}_f^p - \hat{\boldsymbol{\psi}}_h^p,$$

that are obtained by solving the dual Problem (16).

Proposition 3.5 *From the previous error representation, we derive the following approximate error estimate*

$$|J(\hat{\mathbf{U}}) - J(\hat{\mathbf{U}}_h)| \approx \sum_{\widehat{K} \in \hat{\mathcal{T}}_h} \eta_{\widehat{K}}, \quad \eta_{\widehat{K}} := \sum_{i=1}^7 \rho_K^{(i)} \omega_K^{(i)},$$

with the residual terms and the weights

$$\begin{aligned} \rho_K^{(1)} &:= \| -\hat{\rho}_f \hat{\mathbf{J}}(\widehat{\mathbf{F}}^{-1} \hat{\mathbf{v}}_f \cdot \widehat{\boldsymbol{\nabla}}) \hat{\mathbf{v}}_f + \widehat{\boldsymbol{\nabla}} \cdot \widehat{\boldsymbol{\sigma}}_{appr} - \widehat{\boldsymbol{\nabla}} \hat{\rho}_f \|_{\widehat{K}}, & \omega_K^{(1)} &:= \| \hat{\mathbf{z}}_f^v - \hat{\boldsymbol{\psi}}_h^v \|_{\widehat{K}}, \\ \rho_K^{(2)} &:= \| \widehat{\boldsymbol{\nabla}} \cdot \widehat{\boldsymbol{\Sigma}}_{appr} \|_{\widehat{K}}, & \omega_K^{(2)} &:= \| \hat{\mathbf{z}}_s^v - \hat{\boldsymbol{\psi}}_h^v \|_{\widehat{K}}, \\ \rho_K^{(3)} &:= \| \widehat{\boldsymbol{\nabla}} \cdot \widehat{\boldsymbol{\sigma}}_{mesh} \|_{\widehat{K}}, & \omega_K^{(3)} &:= \| \hat{\mathbf{z}}_f^u - \hat{\boldsymbol{\psi}}_h^u \|_{\widehat{K}}, \\ \rho_K^{(4)} &:= \| \widehat{\mathbf{div}}(\hat{\mathbf{J}} \widehat{\mathbf{F}}^{-1} \hat{\mathbf{v}}_f) \|_{\widehat{K}}, & \omega_K^{(4)} &:= \| \hat{\mathbf{z}}_f^p - \hat{\boldsymbol{\psi}}_h^p \|_{\widehat{K}}, \\ \rho_K^{(5)} &:= \frac{1}{2} \hat{h}_K^{-1/2} \| [\hat{\mathbf{J}} \widehat{\boldsymbol{\sigma}}_f \widehat{\mathbf{F}}^{-T} \hat{\mathbf{n}}_f] \|_{\partial \widehat{K} \cup \widehat{\Gamma}_i}, & \omega_K^{(5)} &:= \frac{1}{2} \hat{h}_K^{1/2} \| \hat{\mathbf{z}}_f^v - \hat{\boldsymbol{\psi}}_h^v \|_{\partial \widehat{K} \cup \widehat{\Gamma}_i}, \\ \rho_K^{(6)} &:= \frac{1}{2} \hat{h}_K^{-1/2} \| [\widehat{\mathbf{F}} \widehat{\boldsymbol{\Sigma}}_{appr} \hat{\mathbf{n}}_s] \|_{\partial \widehat{K} \cup \widehat{\Gamma}_i}, & \omega_K^{(6)} &:= \frac{1}{2} \hat{h}_K^{1/2} \| \hat{\mathbf{z}}_s^v - \hat{\boldsymbol{\psi}}_h^v \|_{\partial \widehat{K} \cup \widehat{\Gamma}_i}, \\ \rho_K^{(7)} &:= \frac{1}{2} \hat{h}_K^{-1/2} \| [\widehat{\boldsymbol{\sigma}}_{mesh} \hat{\mathbf{n}}_f] \|_{\partial \widehat{K} \cup \widehat{\Gamma}_i}, & \omega_K^{(7)} &:= \frac{1}{2} \hat{h}_K^{1/2} \| \hat{\mathbf{z}}_f^u - \hat{\boldsymbol{\psi}}_h^u \|_{\partial \widehat{K} \cup \widehat{\Gamma}_i}. \end{aligned}$$

The weights $\omega^{(i)}$ are approximated by post-processing of the discrete dual solution.

A mesh adaptation algorithm

Let an error tolerance TOL be given. Local error indicators from an a posteriori error estimate on the mesh $\hat{\mathcal{T}}_h$ are extracted to realize the mesh adaption:

$$|J(\hat{\mathbf{U}}) - J(\hat{\mathbf{U}}_h)| \leq \eta := \sum_{\widehat{K} \in \hat{\mathcal{T}}_h} \eta_{\widehat{K}} \quad \text{for all cells } \widehat{K} \in \hat{\mathcal{T}}_h.$$

This information is used to adapt the mesh using the following strategy:

1. Compute the primal solution \hat{U}_h and the dual solution \hat{Z}_h on the present mesh $\hat{\mathcal{T}}_h$.
 2. Determine the cell indicator $\eta_{\hat{K}}$ at each cell \hat{K} .
 3. Compute the sum of all indicators $\eta := \sum_{\hat{K} \in \hat{\mathcal{T}}_h} \eta_{\hat{K}}$.
 4. Check, if the stopping criterion is satisfied: $|J(\hat{U}) - J(\hat{U}_h)| \leq \eta \leq TOL$, then accept \hat{U}_h within the tolerance TOL . Otherwise, proceed to the following step.
 5. Mark all cells \hat{K}_i that have values $\eta_{\hat{K}_i}$ above the average $\frac{\alpha\eta}{N}$ (where N denotes the total number of cells of the mesh \mathbb{T}_h and $\alpha \approx 1$).
- Other mesh adaption strategies are discussed in [16, 42].

4. Numerical Tests

We discuss two numerical examples that are based on the same configuration and parameters. These data are taken from the literature and were discussed with a cardiologist. The tests are simulated with the software package deal.II [43, 44].

The (reference) configuration $\hat{\Omega}$ of both test cases is illustrated in Fig. 1.

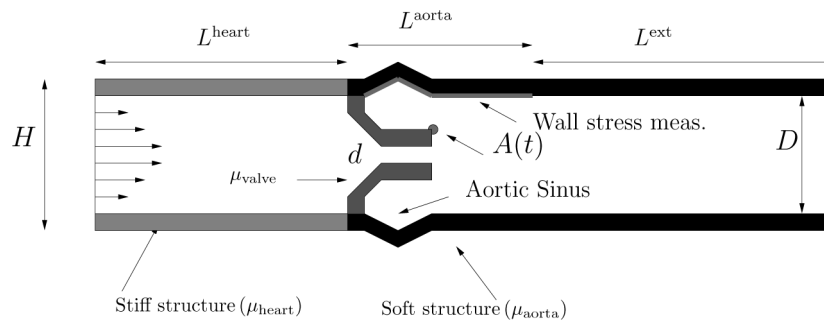


Fig. 1. Configuration of the heart-valve setting for adaptive mesh refinement

We are dealing with a coupling of Newtonian fluid flows with multiple structures. The structure is divided into three different sub-structures by changing the material parameters. Specifically, the part L^{heart} is characterized by high stiffness. The material in the middle part L^{aorta} is much smoother, whereas the last part L^{ext} is used to absorb the energy utilizing the structural damping.

Configuration

The (reference) configuration $\hat{\Omega}$ of the test case is illustrated in Fig. 1. The principal dimensions for the stationary test case are $L^{\text{heart}} + L^{\text{aorta}} = 6.0 \text{ cm}$,

$L^{\text{ext}} = 3\text{cm}$, $H = 2.9\text{cm}$, $D = 2.5\text{cm}$, $d = 0.1\text{cm}$. In the second test below, the artificial domain is prolonged, such that $L^{\text{ext}} = 9\text{cm}$ [7, 8].

4.1. Results of Test 1

This part is motivated to quantify different mesh refinement techniques for stationary heart-valve simulations.

Inflow and boundary conditions

A parabolic constant inflow velocity profile is prescribed on $\widehat{\Gamma}_{\text{in}}$:

$$v_f(0, y) = \widehat{v}^D \frac{(y - D/2)(y + D/2)}{0.25D^2}, \quad \widehat{v}^D = 10^{-2}\text{cm/s},$$

leading to a steady-state solution. The do-nothing condition is used on $\widehat{\Gamma}_{\text{out}}$ (right boundary D in Fig. 1).

The structure is fixed on $\widehat{\Gamma}_{\text{in}}$ and $\widehat{\Gamma}_{\text{out}}$ and it is left free at the outer elastic walls, to allow them to move (however, in this test case, we do not expect large deformations of the outer structure).

Quantities of comparison and their evaluation

We evaluate the deflections in both the x - and the y -directions at the tail of the upper valve at the point $A(0) = (3.64, 0.35)$. In the first test case, the y -deflection of this point is taken as goal functional for mesh refinement with the DWR method (see Example 3.1 for its evaluation). In the second example, we take the line integral of the wall stresses as goal functional, which is computed along the interface of the aorta and the blood (see Example 3.2 for its evaluation).

Table 1.

The displacements of the control point A for a sequence of mesh levels of locally refined meshes with the DWR method. The goal functional is given by the y -component of the point A .

The reference value is obtained on a globally refined mesh (last row)

Cells	DoF	$A(x)[10^{-4}\text{cm}]$	$A(y)[10^{-4}\text{cm}]$
188	3996	2.6153	8.7667
233	5136	2.6921	9.1156
479	10556	2.7576	9.1793
926	20232	2.7674	9.1706
1721	37484	2.7700	9.1636
2882	62912	2.7742	9.1629
4685	101804	2.7763	9.1621
12032	242500	2.7651	9.1538

Parameters

For the fluid, we use the density $\rho_f = 1 \text{ gcm}^{-3}$, and the viscosity $\nu_f = 0.03 \text{ cm}^2 \text{ s}^{-1}$. The elastic structure is characterized by the density $\rho_s = 1 \text{ gcm}^{-3}$, the Poisson ratio $\nu_s = 0.3$, and the Lamé coefficients $\mu_{\text{heart}} = 10^8 \text{ gcm}^{-1} \text{ s}^{-2}$, $\mu_{\text{valve}} = 5.0 * 10^5 \text{ gcm}^{-1} \text{ s}^{-2}$, $\mu_{\text{aorta}} = 10^6 \text{ gcm}^{-1} \text{ s}^{-2}$, and $\mu_{\text{ext}} = 10^6 \text{ gcm}^{-1} \text{ s}^{-2}$. We remind the reader that the adjustment of the both damping parameters is redundant because $\hat{\nu}_s = 0$ and therefore, the damping terms vanish anyway.

Discussion of the results for the point value evaluation

The deflections in both principal directions are displayed for a sequence of locally refined meshes with the DWR method in Table 1. A comparison between the three proposed refinement types can be observed in Fig. 2. The reference value for the error determination is computed on a very fine mesh obtained with global refinement and extrapolation of the solution. We monitor the same convergence rate for both global refinement and local mesh adaption with the DWR method. However, as expected, we detect a better constant when using the DWR method. The heuristic indicator performs worse than the other two procedures and should not be used for rigorous a posteriori mesh adaption in this numerical example. The corresponding meshes are displayed in Fig. 3 for solutions on three different mesh levels.

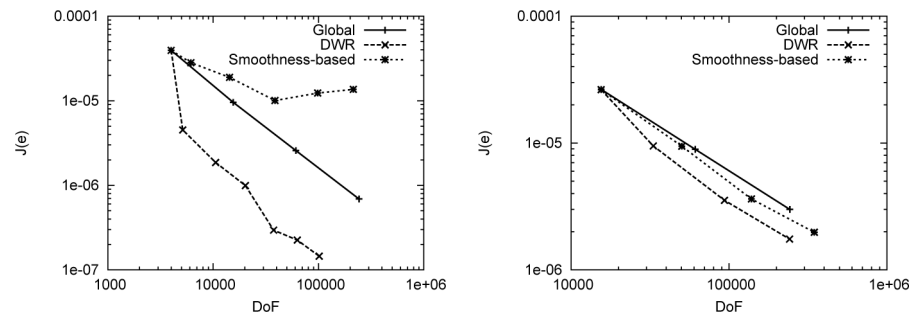


Fig. 2. Error of the point y -evaluation at the tail A of the upper valve (left) and the wall stress evaluation (right) versus number of degrees of freedom, for uniform refinement, the weighted indicator obtained with the DWR method, and smoothness-based indicators. For both goal functionals the DWR method performs best. For wall stress measurement the smoothness-based refiner also beats global mesh refinement

Discussion of the results for the wall stress evaluation

In addition to the previous statements, we observe that both the DWR method and the heuristic mesh refiner beat global mesh refinement in the second test case. The corresponding meshes of the DWR method are displayed in Fig. 4 for solutions on three different mesh levels. The good performance

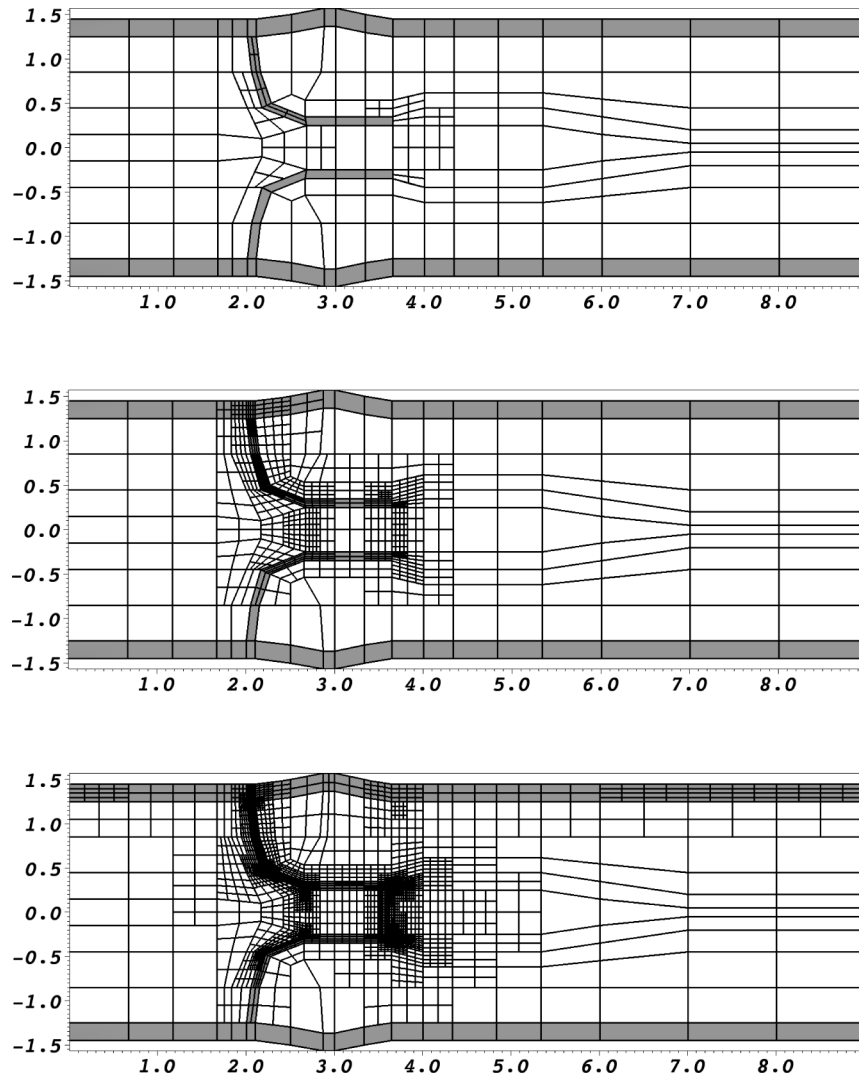


Fig. 3. Meshes with 233, 926, and 4685 cells obtained with the DWR estimator for the point y -evaluation at A as target functional. The unit of the both axes is cm

of the smoothness-based refinement for the computation of the wall stresses is exploited for the nonstationary examples in Section 4.2.

4.2. Results of Test 2

In the second numerical test, the flow is driven with the help of a time-dependent inflow profile (see Fig. 5) leading to pulsatile flow in a laminar regime.

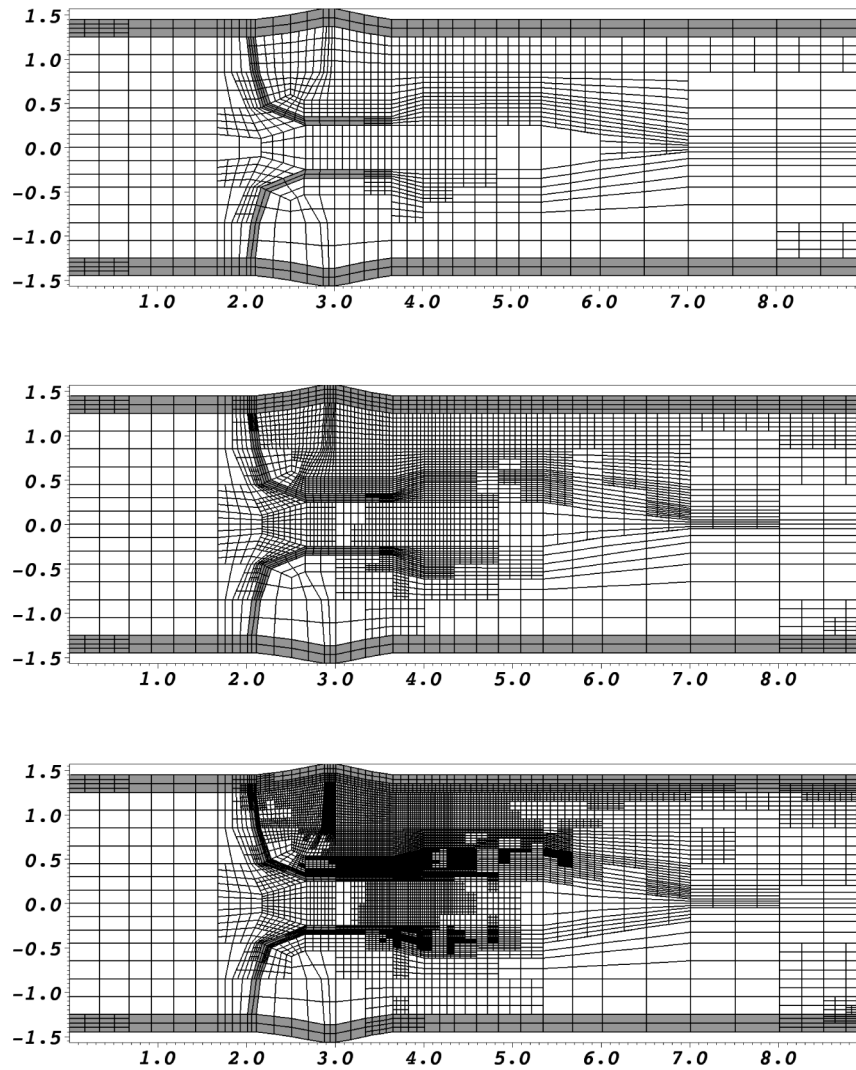


Fig. 4. Meshes with 1580, 4496, and 11636 cells obtained with the DWR estimator for the wall stress evaluation along the interface of L^{aorta} as target functional. The unit of the both axes is *cm*

The goal of this test is to test local mesh refinement for nonstationary heart-valve dynamics. To this end, the valves have sufficient distance to avoid touching and induced difficulties.

One cardiac cycle has time length $T = [0s, 0.9s]$. Four time cycles are used to run the computation. The time step sizes are chosen in a range of $t = 0.02s - 0.002s$ to detect convergence with respect to time. The results are obtained for four different refinement levels, i.e., 5553, 21522, 84726, and 145,206 degrees of freedom. A deeper discussion of the influence of

different choices for the damping parameters, various lengths of the artificial layer, etc., is studied in [7, 8].

Inflow and boundary conditions

A time-dependent parabolic velocity inflow profile is prescribed on $\hat{\Gamma}_{in}$ (left boundary H), sketched in Fig. 5, for the first test case. This inflow profile is scaled with a constant factor 0.1.

The ‘do-nothing’ condition is used on $\hat{\Gamma}_{out}$ (right boundary D in Fig. 1).

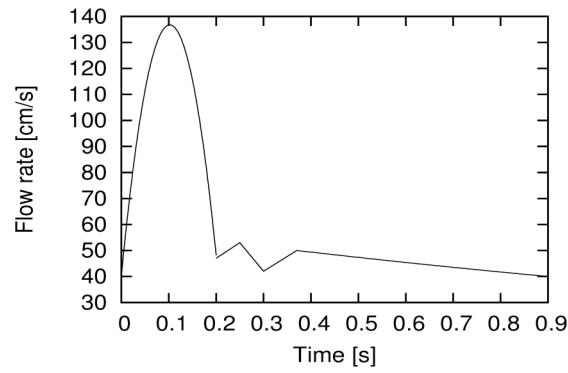


Fig. 5. Interpolated flow rate profile $\bar{v}(t)$ in one cardiac cycle that is used to scale the inflow profile

The structure is fixed at $\hat{\Gamma}_{in}$ and $\hat{\Gamma}_{out}$ and it is left free at the outer elastic walls, to allow them to move.

Quantities of comparison and their evaluation

We evaluate the deflections in both x - and y -directions at the tail of the upper valve at the point $A(0) = (3.64, 0.35)$, and the wall stresses at the upper wall between the fluid and the structure in the aorta (over the length L^{aorta}).

Parameters

For the fluid, we use the density $\rho_f = 1 \text{ gcm}^{-3}$, and the viscosity $\nu_f = 0.03 \text{ cm}^2 \text{ s}^{-1}$. The elastic structure is characterized with the density $\rho_s = 1 \text{ gcm}^{-3}$, the Poisson ratio $\nu_s = 0.3$, and the Lamé coefficients $\mu_{heart} = 10^8 \text{ gcm}^{-1} \text{ s}^{-2}$, $\mu_{valve} = 5.0 * 10^5 \text{ gcm}^{-1} \text{ s}^{-2}$, $\mu_{aorta} = 10^6 \text{ gcm}^{-1} \text{ s}^{-2}$. The (weak) damping parameter is given by $\gamma_w = 10^4$, the other one $\gamma_s = 0$.

In Fig. 6, we observe the qualitative behavior of the physical quantities for the last three cardiac cycles.

Two time step solutions on a locally refined mesh within one cardiac cycle can be studied in Fig. 8. We use local mesh adaption with refinement indicators that are obtained by smoothness measurement of the discrete solutions (see (12)). As shown in Section 4.1, the heuristic mesh refinement procedure is an adequate tool (at least) to computing the wall stresses. This

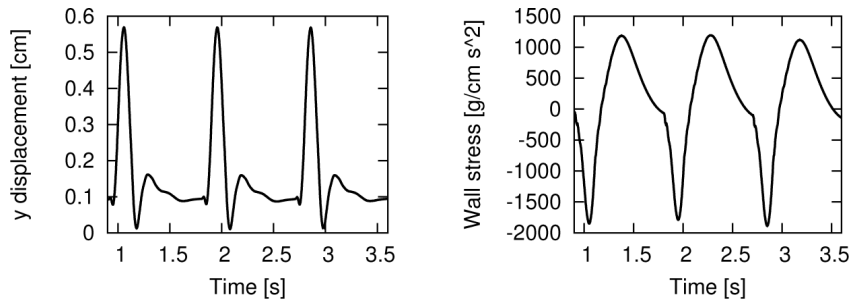


Fig. 6. Nonstationary heart-valve interaction with local mesh refinement: evaluation of the y -displacement at $A(t)$ and the wall stress in the y -direction along the upper wall of L^{aorta}

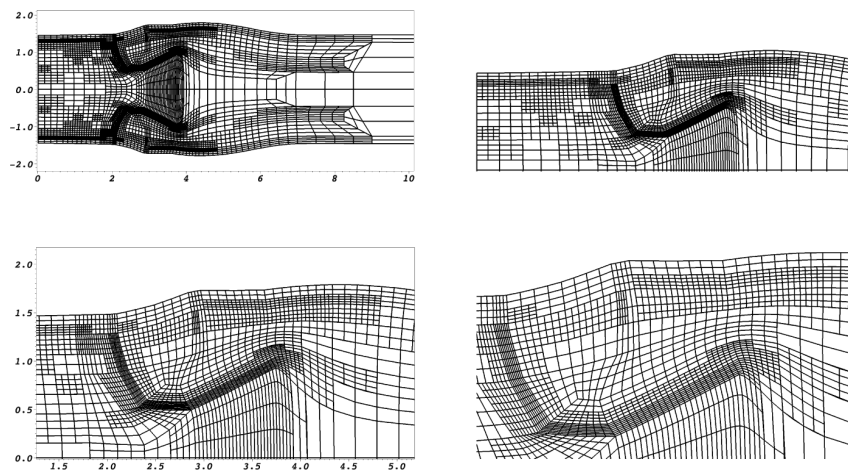


Fig. 7. Nonstationary valve simulation on a three-times locally refined mesh with 145,206 degrees of freedom. The indicators for the mesh refinement are obtained with smoothness measurement of the discrete solution. Specifically, the mesh is mainly refined in the region of interest and not in the artificial layer, which can be seen in the top left figure. By zooming into the mesh (bottom right), we observe a good mesh quality. This is mainly due to the biharmonic mesh motion model. The scales of the both axes are given in cm

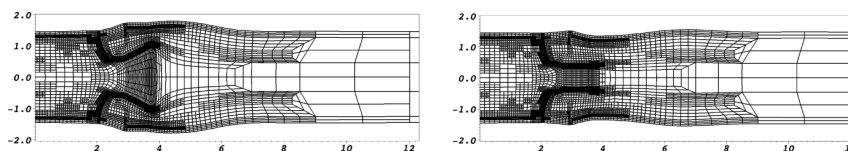


Fig. 8. Two time steps $t = 0.994$ and 1.020 (in s) on a locally refined mesh of the nonstationary heart-valve simulations within one cardiac cycle. Specifically, the mesh is mainly refined in the physical domain $L = 6cm$. The unit of the both axes is cm

are good news, because the computation of wall stresses might be important for clinical applications, whereas the point value evaluation, where smoothness-based refinement failed, is only considered for numerical studies.

As we monitor in Fig. 7, the mesh refiner is able to refine along the interfaces of interest (namely along L^{aorta}) and, in addition, it only refines the mesh in the physical region of interest but not in the artificial layer.

5. Conclusions

In this work, we proposed adaptive mesh refinement concepts for monolithic fluid-structure interaction with application to a prototypical aortic heart-valve setting. For the nonstationary simulations, the computational domain was prolonged with an artificial layer to prevent backflow of structure waves. To reduce the higher computational cost, we developed a DWR estimator for mesh adaption. Specifically, our estimators for adaptive mesh refinement were able to refine the mesh along an interface-section for wall stress measurement. We plan to extend the DWR approach to time-dependent cases. Moreover, we plan to extend the DWR method to sophisticated structure models, which account for pre-stressed configurations. Finally, we have 3D simulations in mind for which we must use efficient mesh refinement techniques.

Acknowledgments

The financial support by the DFG (Deutsche Forschungsgemeinschaft) and the HGS MathComp Heidelberg is gratefully acknowledged. Furthermore, the author thanks Dr. med. Jeremi Mizerski for fruitful discussions.

Manuscript received by Editorial Board, June 16, 2011;
final version, April 05, 2012.

REFERENCES

- [1] Quarteroni A.: What mathematics can do for the simulation of blood circulation. MOX Report, 2006.
- [2] Figueroa C.A., Vignon-Clementel I.E., Jansen K.E., Hughes T.J.R., Taylor C.A.: A coupled momentum method for modeling blood ow in three-dimensional deformable arteries. *Comput. Methods Appl. Mech. Engrg.*, 2006, Vol. 195, pp. 5685-5706.
- [3] Nobile F., Vergara C.: An Effective Fluid-Structure Interaction Formulation for Vascular Dynamics by Generalized Robin Conditions. *SIAM J. Sci. Comput.*, 2008, Vol. 30, No. 2, pp. 731-763.
- [4] Janela J., Moura A., Sequeira A.: Absorbing boundary conditions for a 3D non-Newtonian fluid-structure interaction model for blood flow in arteries. *Int. J. Engrg. Sci.*, 2010.

- [5] Formaggia L., Quarteroni A., Veneziani A.: *Cardiovascular Mathematics: Modeling and simulation of the circulatory system*, Springer-Verlag, Italia, Milano, 2009.
- [6] Formaggia L., Veneziani A., Vergara Ch.: Flow rate boundary problems for an incompressible fluid in deformable domains: formulations and solution methods. *Comput. Meth. Appl. Mech. Engrg.*, 2010, Vol. 199, pp. 677-688.
- [7] Wick T.: An energy absorbing layer for the structure outflow boundary for fluid-structure interactions applied to valve dynamics, in review, 2011.
- [8] Wick T.: Adaptive finite element simulation of fluid-structure interaction with application to heart valve dynamics, PhD thesis, 2011.
- [9] Jianhai Z., Dapeng C., Shengquan Z.: ALE finite element analysis of the opening and closing process of the artificial mechanical valve. *Applied Math. Mech.*, 2006, Vol. 17, No. 5, pp. 403-412.
- [10] Le Tallec P., Mouro J.: Fluid structure interaction with large structural displacements. *Comput. Meth. Appl. Mech. Engrg.*, 2001, Vol. 190, pp. 3039-3067.
- [11] Peskin C.: The immersed boundary method. *Acta Numerica*, Cambridge University Press, 2002, pp. 1-39.
- [12] Diniz Dos Santos N., Gerbeau J.-F., Bourgat J.F.: A partitioned fluid-structure algorithm for elastic thin valves with contact. *Comp. Meth. Appl. Mech. Engrg.*, 2008, Vol. 197, No. 19-20, pp. 1750-1761.
- [13] Vierendeels J., Dumont K., Verdonck P.R.: A partitioned strongly coupled fluid-structure interaction method to model heart valve dynamics. *J. Comp. Appl. Math.*, 2008.
- [14] Baaijens F.P.T.: A fictitious domain/mortar element method for fluid-structure interaction, *Int. J. Num. Methods Fluids*, 2001, Vol. 35, pp. 743-761.
- [15] Causin P., Gerbeau J.-F., Nobile F.: Added-mass effect in the design of partitioned algorithms for fluid-structure problems. *Comput. Methods Appl. Mech. Engrg.*, 2005, Vol. 194, pp. 4506-4527.
- [16] An optimal control approach to error control and mesh adaptation in finite element methods. *Acta Numerica 2001*, (A. Iserles, ed.), Cambridge University Press, 2001.
- [17] Dunne T.: An Eulerian approach to fluid-structure interaction and goal-oriented mesh adaptation, *Int. J. Numer. Methods in Fluids*, 2006, Vol. 51, pp. 1017-1039.
- [18] Numerical Simulation of Fluid-Structure Interaction Based on Monolithic Variational Formulations. *Numerical Fluid Structure Interaction*, G.P. Galdi, R. Rannacher et. al, Springer, 2010.
- [19] Richter T.: Goal oriented error estimation for fluid-structure interaction problems, *Computer Methods in Applied Mechanics and Engineering* 223-224, pp. 38-42, 2012.
- [20] van der Zee K.G., van Brummelen E.H., de Borst R.: Goal-oriented error estimation for Stokes flow interacting with a flexible channel. *Int. J. Numer. Meth. Fluids*, 2008, Vol. 56, pp. 1551-1557.
- [21] Bathe K.-J., Grätsch T.: Goal-oriented error estimation in the analysis of fluid flows with structural interactions. *Comp. Methods Appl. Mech. Engrg.*, 2006, Vol. 195, pp. 5673-5684.
- [22] Fung Y.C.: *Biodynamics: Circulation*, first ed., Springer-Verlag, 1984.
- [23] Holzapfel G.A.: *Nonlinear Solid Mechanics: A continuum approach for engineering*, John Wiley and Sons, LTD, 2000.
- [24] Holzapfel G.A., Ogden R.W.: *Mechanics of Biological Tissue*, Springer, Heidelberg, 2006.
- [25] Humphrey J.D.: *Cardiovascular Solid Mechanics: Cells, Tissues, and Organs*, Springer, New York, 2002.
- [26] Wloka J.: *Partielle Differentialgleichungen*, B.G. Teubner, Stuttgart, 1987.
- [27] Berenger J.-P.: A perfectly matched layer for the absorption of electromagnetic waves. *J. Comput. Phys.*, 1994, Vol. 114, No. 185.

- [28] Formaggia L., Moura A., Nobile F.: On the stability of the coupling of 3D and 1D fluid-structure interaction models for blood flow simulations. Technical Report at MOX, 2006, Vol. 94.
- [29] Vignon-Clementel I.E., Figueroa C.A., Jansen K.E., Taylor Ch.A.: Outflow boundary conditions for three-dimensional finite element modeling of blood flow and pressure in arteries. *Comput. Meth. Appl. Mech. Engrg.*, 2006, Vol. 195, pp. 3776-3796.
- [30] Stein K., Tezduyar T., Benney R.: Mesh moving techniques for fluid-structure interactions with large displacements, *J. Appl. Math.*, 2003, Vol. 70, pp. 58-63.
- [31] Tezduyar T. E., Behr M., Mittal S., Johnson A. A.: Computation of Unsteady Incompressible Flows With the Finite Element MethodsSpace- Time Formulations, Iterative Strategies and Massively Parallel Implementations. *ASME: New Methods in Transient Analysis*, 1992, Vol. 143, pp. 7-24.
- [32] Wick T.: Fluid-Structure Interactions using Different Mesh Motion Techniques, *Comput. Struct.*, 2011, Vol. 89, pp. 1456-1467.
- [33] Brooks A. N., Hughes T. J. R.: Streamline upwind/Petrov-Galerkin formulations for convection dominated flows with particular emphasis on the incompressible Navier-Stokes equations, *Comput. Methods Appl. Mech. Engrg.*, 1982, Vol. 32, No. 1-3, pp. 199-259.
- [34] Wall Wolfgang A.: Fluid-Struktur-Interaktion mit stabilisierten Finiten Elementen, PhD Thesis, University of Stuttgart, 1999.
- [35] Braack M., Burman E., John V., Lube G.: Stabilized finite element methods for the generalized Oseen equations. *Comput. Methods Appl. Mech. Engrg.*, 2007, Vol. 196, No. 4-6, pp. 853-866.
- [36] Besier M.: Adaptive Finite Element methods for computing nonstationary incompressible Flows, University of Heidelberg, 2009.
- [37] Besier M., Wollner W.: On the dependence of the pressure on the time step in incompressible flow simulations on varying spatial meshes, *Int. J. Num. Methods in Fluids*, 2011.
- [38] Becker R., Rannacher R.: A feed-back approach to error control in finite element methods: basic analysis and examples. *East-West J. Numer. Math.*, 1996, Vol. 4, pp. 237-264.
- [39] Wick T.: Adaptive Finite Elements for Fluid-Structure Interactions on a Prolongated Domain: Applied to Valve Simulations, *Proc. Comput. Methods Mech.*, Warsaw in Poland, May 9-12, 2011.
- [40] Zienkiewicz O.C., Zhu J.Z.: The superconvergent patch recovery and a posteriori error estimates. Part 1: The recovery technique, *Int. J. of Numer. Methods Engrg.*, 1992, Vol. 33, pp. 1331-1364.
- [41] Zienkiewicz O.C., Zhu J.Z.: The superconvergent patch recovery and a posteriori error estimates. Part 2: Error estimates and adaptivity, *Int. J. of Numer. Methods Engrg.*, 1992, Vol. 33, pp. 1365-1382.
- [42] Bangerth W., Rannacher R.: Adaptive Finite Element Methods for Differential Equations. *Lectures in Mathematics*, ETH Zuerich, Birkhäuser Verlag, 2003.
- [43] Bangerth W., Hartmann R., Kanschat G.: Differential Equations Analysis Library. Technical Reference, 2010. <http://www.dealii.org>
- [44] Wick T.: Solving Monolithic Fluid-Structure Interaction Problems in Arbitrary Lagrangian Eulerian Coordinates with the deal.II Library. IWR-Preprint, 2011, in review for publication in *Archive of Numerical Software*.
- [45] Heywood J., Rannacher R., Turek S.: Artificial boundaries and flux and pressure conditions for the incompressible Navier-Stokes equations. *Int. J. Num. Meth. Fluids.*, 1996, Vol. 22, pp. 325-353.

Metody adaptacji siatki w zagadnieniu oddziaływania płyn-struktura (FSI) w zastosowaniu do symulacji przepływu przez zastawkę serca**Streszczenie**

W artykule przedstawiono analizę zagadnienia oddziaływania płyn-struktura (FSI) w komputerowej symulacji pracy zastawki serca. Przedstawiono monolityczne sformułowanie tego zagadnienia, w którym równania dla struktury i płynu rozwiązywane są w pełnym sprzężeniu, przy czym do opisu ruchu płynu stosowane jest podejście typu Arbitrary Lagrangian-Eulerian (ALE). Zaproponowano metodę eliminacji zjawiska niefizycznego odbicia fal odkształceń struktury, polegającą na wprowadzeniu sztucznej dyssypacji energii tych fal w części brzegu obszaru położonej za zastawkami. W celu zwiększenia efektywności obliczeniowej wprowadzono lokalną adaptację siatki. W szczególności, porównano heurystyczne techniki adaptacji siatki z techniką opartą na wykorzystaniu ważonego residuum sprzężonego (Dual Weighted Residual, DWR). Przedstawiono wyniki obliczeń testowych demonstrujące poprawność zaproponowanego podejścia oraz skuteczność metody adaptacyjnej DWR.